

Article

N-Doped Nanocrystalline Graphite Electrochemical Sensor for Oleuropein Detection from Extra Virgin Olive Oils

Camelia Albu ¹, Ana Chira ¹, Alice Stoica ¹, Gabriel-Lucian Radu ¹, Antonio Radoi ², Marius Stoian ², Octavian-Gabriel Simionescu ² and Sandra A. V. Eremia ^{1,*}

¹ National Institute of Research and Development for Biological Sciences, 060031 Bucharest, Romania; camelia.albu@incdsb.ro (C.A.); ana.chira@incdsb.ro (A.C.); alice.stoica@incdsb.ro (A.S.); lucian.radu@incdsb.ro (G.-L.R.)

² National Institute for Research and Development in Microtechnologies—IMT Bucharest, 077190 Voluntari, Romania; antonio.radoi@imt.ro (A.R.); marius.stoian@imt.ro (M.S.); octavian.simionescu@imt.ro (O.-G.S.)

* Correspondence: sandra.eremia@incdsb.ro

Abstract: A nitrogen-doped nanocrystalline electrochemical graphite sensor for the sensitive determination of oleuropein (OL) from extra virgin olive oils (EVOOs) is presented. The sensor was developed by the deposition of nanocrystalline graphite (NCG) using plasma-enhanced chemical vapour deposition (PECVD) on silicon wafers. Scanning electron microscopy (SEM), energy dispersive X-ray analysis (EDX) and X-ray diffraction analysis (XRD) were used to characterise the microstructure and morphology of the developed materials. Cyclic voltammetry (CV), electrochemical impedance spectroscopy (EIS) and square wave voltammetry (SWV) were used to investigate the electrochemical properties of the material and the performance of the sensor. The developed sensor showed good analytical performance against OL over a concentration range of 5.00–500.00 μM , with a good detection limit of 3.93 μM and a good sensitivity of 0.057 $\mu\text{A } \mu\text{M}^{-1}$. The reproducibility of the electrochemical sensor was excellent, with a relative standard deviation (RSD) of 8.56% for seven measurements.

Keywords: nanocrystalline graphite; electrochemical sensor; square wave voltammetry; oleuropein; extra virgin olive oil



Citation: Albu, C.; Chira, A.; Stoica, A.; Radu, G.-L.; Radoi, A.; Stoian, M.; Simionescu, O.-G.; Eremia, S.A.V. N-Doped Nanocrystalline Graphite Electrochemical Sensor for Oleuropein Detection from Extra Virgin Olive Oils. *Chemosensors* **2024**, *12*, 144. <https://doi.org/10.3390/chemosensors12080144>

Received: 18 June 2024
Revised: 16 July 2024
Accepted: 22 July 2024
Published: 25 July 2024



Copyright: © 2024 by the authors. Licensee MDPI, Basel, Switzerland. This article is an open access article distributed under the terms and conditions of the Creative Commons Attribution (CC BY) license (<https://creativecommons.org/licenses/by/4.0/>).

1. Introduction

Oleuropein (OL) [1] is a natural compound found mainly in olive leaves, olives and olive oil. It belongs to a group of coumarin-like compounds, the secoiridoids, and is particularly known for its health-promoting properties. Secoiridoids are a group of naturally occurring compounds found predominantly in plants of the *Oleaceae* family [2] and contain an open cyclopentane ring that gives rise to unique functional groups such as aldehydes, alcohols and carboxylic acids. This structural feature contributes to their diverse biological activities. The compound has attracted much attention due to its potential therapeutic properties, including antioxidant [3], anti-inflammatory [4] and antimicrobial activities [5].

Oleuropein, together with other secoiridoids, contributes to the distinctive bitter flavour of extra virgin olive oil (EVOO) and is an indicator of high-quality oil [6]. EVOO contains a higher proportion of oleuropein compared to refined olive oils [7]. The oleuropein content can vary greatly depending on factors such as olive variety, the degree of ripeness, the climate and processing methods [8]. The refining process usually reduces the phenolic content, including oleuropein, resulting in a milder flavour and fewer health benefits. In virgin olive oils, as well as in light and pure olive oils, the oleuropein content is lower compared to EVOOs due to less stringent processing methods, as they are more refined and therefore contain significantly less oleuropein and other phenolic compounds, resulting in

a less bitter flavour and fewer health benefits. To obtain a high-quality EVOO with a high oleuropein content, the olives must be harvested earlier in the season, as the oleuropein content decreases as the fruit ripens [9]. In terms of processing techniques, a higher oleuropein content is achieved through cold pressing and minimal processing, which help retain more oleuropein and other phenolic compounds, in contrast to high-temperature processing and extensive refining, which significantly reduce these compounds [10]. Another extremely important aspect is that freshly produced EVOO has the highest oleuropein content. Over time, the phenolic compounds degrade, so it is best consumed within one to two years of production to maximise health benefits [11].

The adulteration of EVOO is a major problem in the olive oil industry [12], affecting both the quality and the health benefits of the product. Oleuropein, an important phenolic compound in EVOO, plays a crucial role in recognising adulteration. Higher oleuropein levels indicate fresh, minimally processed oil, which is essential for maintaining the oil's beneficial properties. The determination of oleuropein is usually carried out using chromatographic techniques such as high-performance liquid chromatography (HPLC) with an ultraviolet (UV) photodiode array detector (DAD) [13] and a fluorescence detector [14] and liquid chromatography–mass spectrometry (LC-MS) [15,16]. Against this background, it is important to have fast, sensitive, simple and cost-effective methods for the detection of oleuropein in EVOOs.

When searching the Web of Science Core Collection for oleuropein and electrochemical sensors, four articles were available. Cittan et al. developed a glassy carbon electrode (GCE) modified with MWCNT for the determination of oleuropein through accumulation on the prepared MWCNT/GCE [17]. The obtained electrochemical sensor was successfully used for the determination of oleuropein in an olive leaf extract. Another electrochemical sensor based on a graphene oxide pencil graphite electrode was prepared by Gomez et al. and used for the determination of oleuropein in an olive leaf extract [18]. Bounegru et al. developed a tyrosinase-based biosensor based on a screen-printed electrode previously modified with single-walled carbon nanotubes (SPE/SWCNT/Tyr) to detect oleuropein in real EVOO samples [19]. In addition, Mohamadi et al. used an electrochemical DNA biosensor based on the immobilisation of double-stranded deoxy-ribonucleic acid (dsDNA) on the surface of a chitosan-modified carbon paste electrode for the determination of oleuropein in olive leaf extracts [20]. Rojas et al. have developed a new hybrid material based on a screen-printed electrode (SPE) for the sensing of the ortho-diphenols oleuropein (OLEU) and hydroxytyrosol (HYT) in extra virgin olive oil (EVOO) and related samples; the electrochemical performance of the newly developed electrochemical sensors was tested using catechol [21].

Nanocrystalline graphite (NCG) refers to a form of graphite that contains many small crystalline grains or domains, typically in the nanometre range, resulting in an increased defect density and surface area [22,23]. These features influence its mechanical, electrical and chemical properties and make it suitable for various advanced applications. Its unique structural properties, combined with its excellent electrical conductivity and high surface area, make it an ideal candidate for enhancing the performance of sensors used to detect a wide range of chemical and biological analytes [24]. Nanocrystalline graphite offers a versatile and powerful platform for the development of advanced electrochemical sensors [25]. Its unique structural and electronic properties enable high sensitivity [26], fast response times and improved selectivity, making it suitable for a variety of applications in biosensing [27], environmental monitoring [28] and industrial quality control. Ongoing research and development efforts aim to overcome the current challenges and fully exploit the potential of nanocrystalline graphite in electrochemical sensing technologies.

In this work, a N-doped nanocrystalline electrochemical graphite sensor is proposed for the sensitive determination of OL from EVOO. The quantitative determination of OL was carried out with the square wave voltametric method. The results obtained using the electrochemical sensor were compared to those obtained by liquid chromatography–mass spectrometry (LC-MS). The developed nanocrystalline electrochemical graphite sensor

provides a versatile and powerful platform that is a simple, cheap, fast and highly sensitive alternative to existing chromatographic methods.

2. Materials and Methods

2.1. Reagents and Solutions

Oleuropein, potassium chloride, potassium ferricyanide and ethanol were obtained from Sigma-Aldrich/Merck, Darmstadt, Germany. All chemicals were of analytical grade and used without further purification. High-purity deionised water obtained from a Milli-Q system (Millipore, Molsheim, France) was used to prepare all of the aqueous solutions. The stock solution of oleuropein was prepared by dissolving 10 mg of oleuropein in 0.5 mL ethanol. Standard solutions of oleuropein were further prepared in the supporting electrolyte, namely 0.1 M KCl.

2.2. Preparation of Samples

The tested EVOO samples were purchased from the local market or from Greek oil producers. For each EVOO sample, 1 g was weighed and dissolved in 2 mL of 40:10 (*v:v*) ethanol:H₂O.

2.3. Preparation of the Nanocrystalline Graphite Transducer

To obtain nitrogen-doped NCG-type materials, bare 4" n-Si wafers (<100> crystallographic orientation, 525 ± 25 µm thickness and 1–5 Ω·cm electrical resistivity) were used as a substrate for deposition via plasma-enhanced chemical vapour deposition (PECVD). The wafers were introduced into a PECVD reaction chamber and the substrate was heated up to ≈900 °C (15 °C min⁻¹) in an Ar/H₂ atmosphere (12%) and annealed at 1500 mTorr for 15 min. This was followed by a plasma step, which is the main growth step, at an RF discharge power of 100 W in a methane/hydrogen/ammonia atmosphere (60 sccm CH₄/75 sccm H₂/2.1–3.1 sccm NH₃) at 1500 mTorr for 2 h. Once the plasma step was completed, the wafers were thermally treated in the same atmosphere for 30 s to stabilise the surface; then, they were gradually cooled under an Ar/H₂ atmosphere (9 °C/min) and evacuated into the load-lock chamber. The detailed growth mechanism of both the pristine bulk NCG and nitrogen-doped NCG is already presented in our previous work [29].

As some of our previous studies on both undoped [30] and doped [29] bulk NCG films for different electrochemical sensors have shown that the N-doped NCG electrodes have the added advantage of not requiring a preactivation step prior to their use, different ammonia fluxes in the precursor mixture composition were used during the plasma step of the NCG growth process to achieve doping with nitrogen atoms in the graphite lattice at different heteroatom concentrations. The previous experiments on electrochemical sensing applications of nitrogen-doped NCG showed increased sensitivity for the lowest ammonia flow used during growth. Despite an overall lower nitrogen concentration, the electrodes developed at lower NH₃ flow rates exhibited a higher ratio of graphitic to pyridinic and pyrrolic nitrogen and a higher sp²/sp³ carbon hybridisation ratio, which could explain their improved performance [29]. Therefore, the ammonia mass flow controller was used here at its minimum allowed flux, showing some variation in the output of ammonia flow: NNCG1 (2.1–2.3 sccm) and NNCG3 (2.7–3.1 sccm). To further tune the nitrogen-doped NCG, an attempt was made to dilute the added ammonia (3.1 sccm NH₃) in the reaction chamber by increasing the methane and hydrogen gas flows up to 100 sccm CH₄/125 sccm H₂ (NNCG3-diluted) while maintaining the same ratio between them.

For better handling and testing of the N-NCG samples, the 4-inch wafers were diced into 18 mm × 12 mm pieces, which served as independent working electrodes during the characterisation and determination of oleuropein. The electrochemical cell used for the respective measurements provides an aperture diameter of 5 mm² (circular shape) on which the surface of the N-NCG samples is exposed and tested in the electrolyte and analyte solutions (Figure 1).

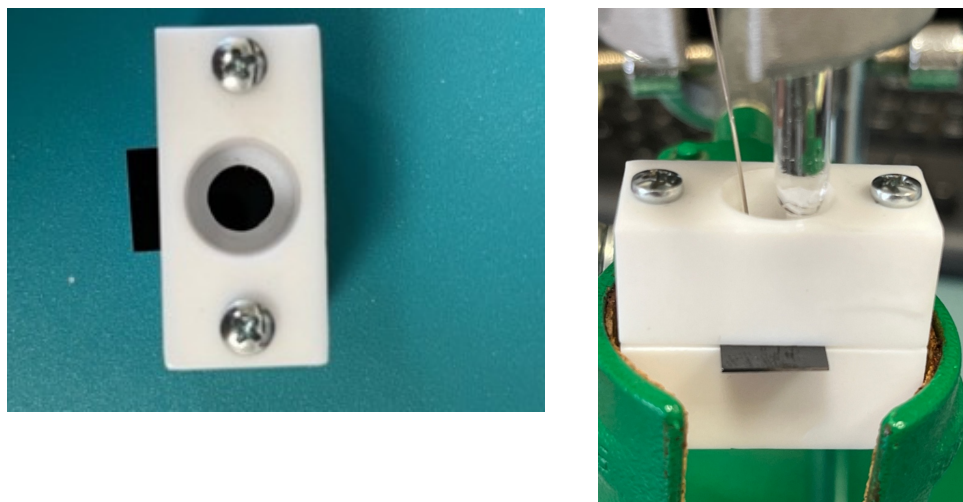


Figure 1. The electrochemical cell used in the experiments.

2.4. Instrumentation and Electrodes

The nitrogen-doped bulk NCG materials were grown with a NANO FAB 1000 system (Oxford Instruments Plasma Technology, Yatton, UK). The surface morphologies of the obtained transducer were characterised using a scanning electron microscope (SEM) (Nova NanoSEM 630, FEI Company, Hillsboro, OR, USA), with an energy-dispersive X-ray spectroscopy (EDX) module (FEI Company, Hillsboro, OR, USA) and an X-ray diffraction (XRD) system with a 9 kW rotating anode, $\text{CuK}_{\alpha 1}$ radiation and $\lambda = 1.5406 \text{ \AA}$ (Rigaku Corporation, Tokyo, Japan) at grazing incidence of 0.5° in the 2θ range of $10\text{--}90^\circ$. The PECVD reaction chamber was NANO FAB 1000 (Oxford Instruments Plasma Technology, Yatton, UK).

The cyclic voltammetry (CV), electrochemical impedance spectroscopy (EIS) and square wave voltammetry (SWV) measurements were carried out using a potentiostat, AutoLab PGSTAT 302N (Metrohm AG, Barendrecht, The Netherlands), that was equipped with the Nova 2.1. Eco Chemie software (Metrohm AG, Barendrecht, The Netherlands). For the EIS measurements, a ground Faraday cage was used to ensure effective shielding against external sources of interference. The electrochemical cell consisted of the nanocrystalline graphite transducer as the working electrode (5 mm diameter, geometric area of 19.635 mm^2), a platinum wire as the counter electrode and Ag/AgCl (3.0 M KCl) as the reference electrode. A standard GC electrode (BioLogic, Seyssinet-Pariset, France, 5 mm electrode diameter, geometric area of 19.635 mm^2) was used for comparison, as it is the most commonly used electrode for electroanalytical detection and has a similar structure to the NCG films presented here.

A Shimadzu chromatograph was used, which consists of an SIL-20AC autosampler, a DGU-20A degassing unit, two LC-20AD pumps, a CTO-20A column oven, LC Solution software var 5.1, an SPDM20A photodiode array detector and an RF-20AXS fluorescence detector.

2.5. Electrochemical Measurements

All CV and SWV measurements were performed at room temperature ($22 \text{ }^\circ\text{C} \pm 0.5 \text{ }^\circ\text{C}$) in batches. The supporting electrolyte consisted of 0.1 M KCl and oleuropein or EVOO samples that were added to the electrochemical cell using a micropipette. The final volume in the electrochemical cell was 0.5 mL . The CV experiments were recorded by cycling the potential between -0.40 and $+0.70 \text{ V}$ at a scan rate of 50 mV s^{-1} . The SWV measurements were performed between $+0.20$ and $+0.70 \text{ V}$ with the following parameters: $a = 50 \text{ mV}$, $f = 25 \text{ Hz}$ and $\Delta E_s = 2 \text{ mV}$.

The EIS experiments were carried out in an equimolar solution of $1 \text{ mM } [\text{Fe}(\text{CN})_6]^{3-} / [\text{Fe}(\text{CN})_6]^{2-}$, which was prepared in 0.1 M KCl . The electrode was polarised at a potential measured by evaluating the free potential (OCP) and an alternating current with 5 mV

amplitude and a frequency range between 9.5 kHz and 0.1 Hz. The results were recorded as a complex plane (Nyquist/Bode). In the EIS measurements, the points are the experimental data, and the lines were determined by interpolation with the classical Randles equivalent circuit.

2.6. HPLC Analysis

The identification and quantification of oleuropein from EVOO samples were performed using a Kromasil 100-5-C18 (Nouryon, Bohus, Sweden) 4.6×250 mm column and a mobile phase consisting of water–acetonitrile (95:5) with 0.2% acetic acid (solvent A) and methanol with 0.2% acetic acid (solvent B), with an elution gradient (0–2 min for 25–60% solvent B, 2–6 min for 60% solvent B, 6.01–10 min for 25% solvent B) and a flow rate of 1 mL min^{-1} .

The experiments were carried out at a constant column temperature of 40°C and an analysis time of 10 min.

The parameters of the fluorescence detector used were as follows: a response time of 1.5 s, 4 gain levels, medium sensitivity, a recording range of 1 and a cell temperature of 25°C . The fluorescence detector was set to the excitation length of $\lambda_{\text{ex}} = 281 \text{ nm}$ and the emission length of $\lambda_{\text{em}} = 316 \text{ nm}$.

3. Results and Discussion

3.1. SEM, EDX and XRD Characterisation

The three samples of the nitrogen-doped NCG material were characterised using SEM, EDX and XRD.

SEM images show the successful deposition of NCG films on the Si substrate which vary in thickness depending on the amount of ammonia used during their growth (Figure 1). The lowest thicknesses are observed for NCG films doped with nitrogen at an ammonia flow of 3.1 sccm, such as NNCG3 (~194 nm) and NNCG3-diluted (~186 nm), due to the additional amount of hydrogen provided from the ammonia molecules that can react with the carbon layer deposited on the substrate, thus consuming the graphitic layers (Figure 2c,e). Therefore, at lower ammonia precursor fluxes, larger thicknesses (~230 nm) are obtained, i.e., NNCG1 (Figure 2a).

There are also differences in the surface morphology of the material depending on the used ammonia flow. NNCG1 (Figure 2b) shows a much more structured appearance with more prominent grains and larger particle sizes (15–20 nm), while the NNCG3 or the diluted NNCG3 samples indicate a finer grain with smaller particles (10–13 nm), which entails a larger specific contact surface.

The nitrogen content of NCG films was estimated by EDX analysis for all growth conditions (Table 1). The lowest heteroatom content in the carbon network of $\approx 0.17\%$ can be observed for the NNCG1 sample, while at a higher ammonia flux during the growth process, the nitrogen content is increased to $\approx 0.37\%$ for NNCG3. Further diluting the ammonia in the reaction chamber by increasing the hydrocarbon and hydrogen flow reduces the nitrogen content that was inserted into the graphitic network to $\approx 0.25\%$ for the NNCG3-diluted sample.

The results in Table 1 show that the average crystallite size increases with the decreasing ammonia volume introduced during the growth process of the NNCG films. The values are 5.17, 3.91 and 3.51 nm for NNCG1, NNCG3-diluted and NNCG3, respectively, in ascending order of heteroatom content in the graphitic network.

The XRD analysis of the three NNCG films shows the presence of graphitic layers with diffraction maxima at $2\theta = 25.83, 43.32$ and 77.95° , next to signals specific to the silicon substrate at $2\theta = 51.18, 53.38$ and 55.59° (Figure 3). The intensity of the diffraction line for the graphite plane (002) at $2\theta = 25.83^\circ$ is higher for the NNCG1 sample than for the NNCG3 sample, indicating a more ordered packing of the graphite layers on extended crystalline domains when the ammonia flux used was limited to lower amounts. At the same time, the diluted ammonia NNCG3 sample shows a pronounced intensity for the

diffraction peak of $2\theta = 25.83^\circ$, indicating a structural similarity to NNCG1. Thus, X-ray diffraction also indicates increased crystallinity for nitrogen-doped NCG films at lower ammonia fluxes in the precursor mixture used in their PECVD growth process, where more graphitic crystalline domains are favoured.

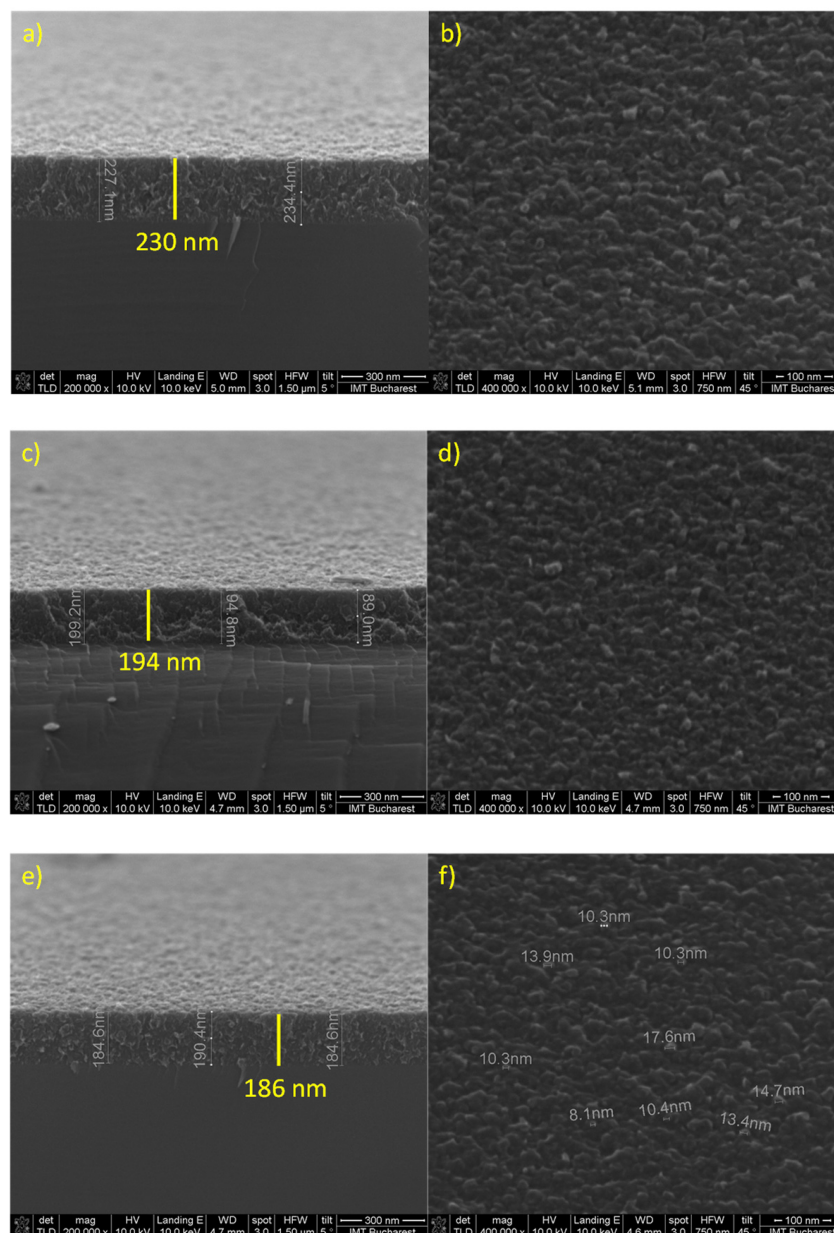


Figure 2. SEM cross-sectional images at different magnifications (200,000 \times and 400,000 \times) of nitrogen-doped NCG-based electrodes deposited on a silicon substrate: NNCG1 (a,b), NNCG3 (c,d) and NNCG3-diluted (e,f).

Table 1. Structural data obtained by EDX analysis.

Sample	NNCG1	NNCG3-Diluted	NNCG3
Nitrogen content (%)	0.17	0.25	0.37
Crystallite size (nm)	5.17	3.91	3.51

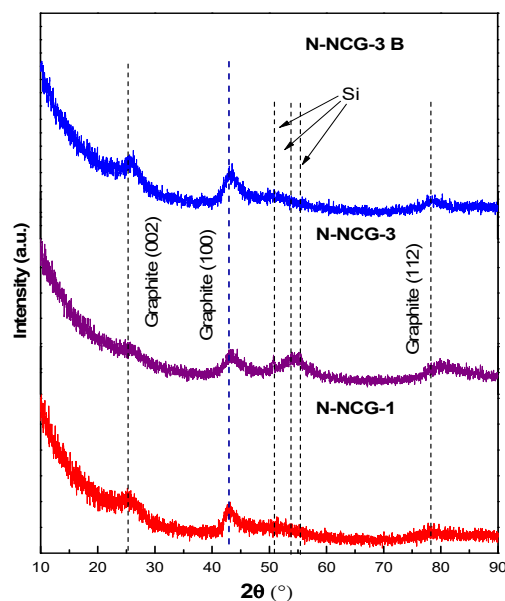


Figure 3. X-ray diffractograms for the samples NNCG1, NNCG3 and NNCG3-diluted.

Using the diffraction peak at $2\theta = 43.3^\circ$ for all NCG-type samples, the average crystallite size was calculated using the Scherrer equation (Equation (1)):

$$D = \frac{K\lambda}{\beta \cos\theta} \quad (1)$$

where D is the average crystallite size, λ is the X-ray wavelength of K_α ($\lambda = 1.5406 \text{ \AA}$), θ is the Bragg diffraction angle and β is the full width at half maximum (FWHM) of the diffraction peak, expressed in radians.

3.2. Electrochemical Behaviour of the NNCG1, NNCG3 and NNCG3-Diluted Transducers

The electrochemical properties of the modified surfaces were investigated by recording the Nyquist impedance spectra. These diagrams are obtained by plotting the imaginary part of the impedance (ZIm) against the real part of the impedance (ZRe). The charge transfer (R_{ct}) at the electrode–electrolyte interface showed significant changes for all functionalised surfaces (Table 2, Figure 4). For comparison, the EIS spectrum of a glassy carbon (GC) electrode (geometric area of 19.635 mm^2 , the same as the NNCG electrode) in the presence of $5 \text{ mM } [\text{Fe}(\text{CN})_6]^{3-/4-}$ with 0.1 M KCl is shown as a reference, as GC is a widely used electrode for electroanalytical detection and has a similar structure to the NCG films presented here.

Table 2. The electrochemical parameters obtained by fitting the EIS data for the tested sensors (R_s —solution resistance, R_{ct} —resistance to charge transfer, Q —element with constant phase, W —Warburg element).

Electrodes	R_s (Ω)	R_{ct} ($\text{k}\Omega$)	W (μS)	Q ($\mu\text{S/n}$)
NNCG1	55.2	1.28	1.72	10.40/0.86
NNCG3	189.0	1.19	1.60	11.20/0.93
NNCG3-dil	34.0	3.58	1.03	8.70/0.83
GC	42.2	0.64	0.55	3.42/0.92

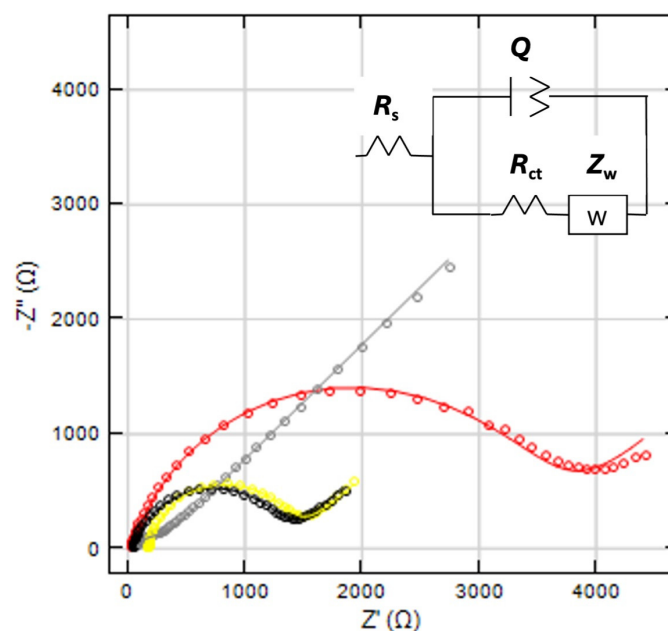


Figure 4. The electrochemical impedance spectra (EIS) recorded for a solution of 5 mM $[\text{Fe}(\text{CN})_6]^{3-/4-}$ in 0.1 M KCl for the modified electrodes NNCG1 (black), NNCG3 (yellow), diluted NNCG3 (red) and GC (grey). Scanning speed, 100 mV s^{-1} . Inset: Randel's equivalent circuit used to fit the EIS data.

All nitrogen-doped nanocrystalline graphite (NNCG) surfaces were tested to analyse the effects of different carbon materials with graphitic structures. The influence of electron density, the variation in the diffusion process and the tracking of the electrical charge transfer process on the modified surfaces were investigated. The electrochemical behaviour was different for each tested transducer.

The NNCG3-diluted transducer showed the highest values of $R_{ct} = 3.58 \text{ k}\Omega$, derived from the diameter of the oblate semicircle in the mid-frequency band. These frequencies determine the resistance to charge transfer that occurs at the electrolyte/graphite substrate and results in limited transport of the analyte molecule. The fitted impedance data for NNCG3 and NNCG1 in Table 2 illustrate the redox capability of these substrates. The lower R_{ct} value of $1.19 \text{ k}\Omega$ indicates better kinetics of the redox reactions on the NNCG3 electrode material. A similar electrochemical behaviour with improved catalytic activity was observed for the NNCG1 electrode.

The bare glassy carbon electrode exhibits low electrocatalytic activity as it is sensitive to the redox probe. According to the results, the electron transport at the bare GC electrode ($R_{ct} = 0.64 \text{ k}\Omega$) was significantly faster. The oxidation/reduction of redox analytes can take place at the bare electrodes with fast redox kinetics. The impedance response of the bare GC electrode shows negligible charge transfer resistance in relation to the conductivity and the geometric surface of the graphitic films.

Furthermore, the electrochemical characterisation of the transducers was further analysed by CV studies using $1 \text{ mM } [\text{Fe}(\text{CN})_6]^{3-/4-}$ in a 0.1 M KCl solution at a scan rate of 50 mV s^{-1} (Figure 5).

The oxidation peak ($E = 350 \text{ mV}$) intensity in the case of NNCG1 ($626 \mu\text{A}$) is 391 times higher than in the case of the classic glassy carbon electrode ($1.60 \mu\text{A}$ at $E = 550 \text{ mV}$). The interesting results obtained for the NNCG1 electrode could be ascribed to a large increase in specific surface area, resulting in an increase in the real electroactive area (roughness factor) and higher conductivity of the modified electrode. The calculated real electroactive area for the NNCG1-modified wafer (circular shape) using a solution of $1 \text{ mM } [\text{Fe}(\text{CN})_6]^{3-/4-}$ in 0.1 M KCl was 1.449 cm^2 (0.37 cm^2 for standard GC); the result reveals that the NNCG1

electrode has a higher electroactive surface area. The more ordered packing of the graphite layers on extended crystalline domains leads to an improved sensitivity.

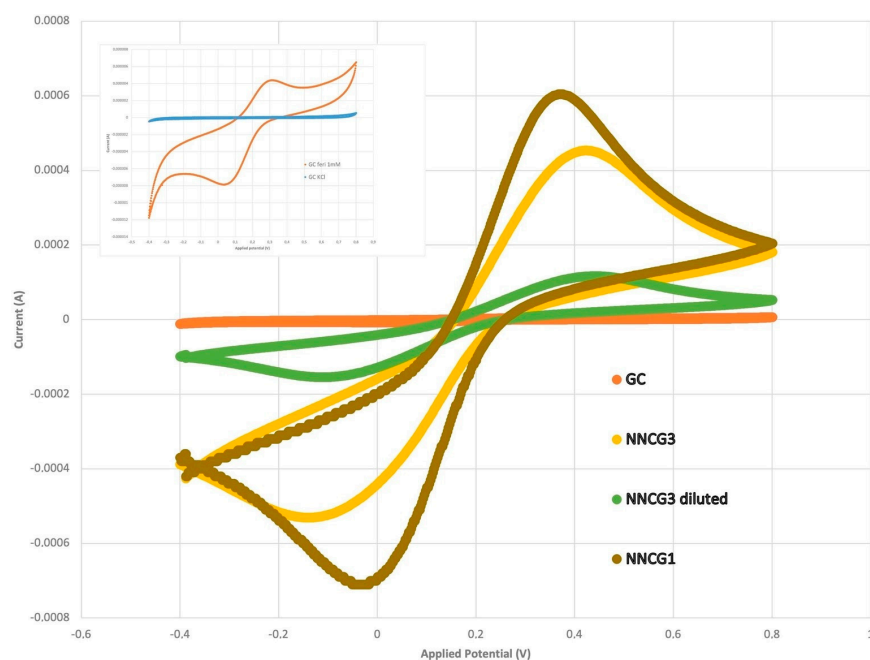


Figure 5. Cyclic voltammograms of $1 \text{ mM } [\text{Fe}(\text{CN})_6]^{3-/4-}$ in 0.1 M KCl solution on NNCG1, NNCG3, NNCG3-diluted 450 and glassy carbon (GC), with scan rate of 50 mV s^{-1} ; cyclic voltammograms of $1 \text{ mM } [\text{Fe}(\text{CN})_6]^{3-/4-}$ in 0.1 M KCl solution on GC (red line) and only KCl (blue line) (inset), with scan rate of 50 mV s^{-1} .

Furthermore, the response of 0.5 mM oleuropein was measured at the surfaces of GC and the three NNCG electrodes in a 0.1 M KCl solution at a scan rate of 50 mV s^{-1} (Figure 6). The mechanism of oleuropein oxidation in an aqueous solution is shown in Scheme 1.

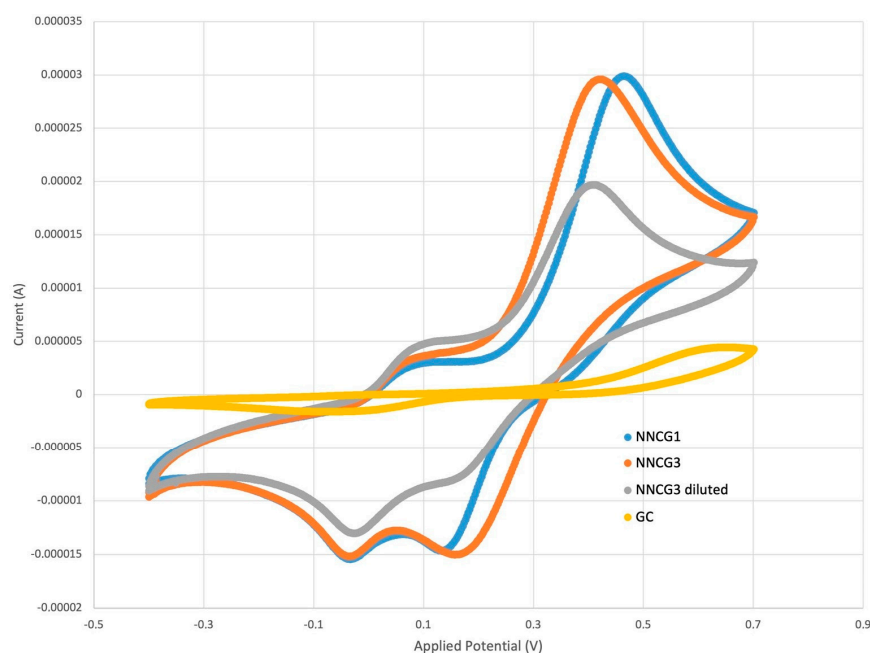
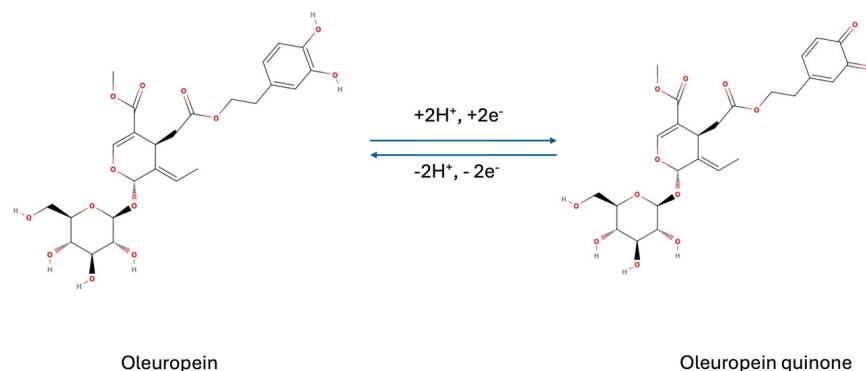


Figure 6. Cyclic voltammograms of 0.5 mM oleuropein in 0.1 M KCl solution on NNCG1, NNCG3, NNCG3-diluted and GC, with scan rate of 50 mV s^{-1} .



Scheme 1. The OL electrochemical reaction process.

Two pairs of quasi-reversible peaks were observed for the NNCG electrodes in the presence of oleuropein. In the case of GC, there is only one pair of quasi-reversible peaks, with the oxidation peak at 600 mV. In the case of NNCG1 and NNCG3, the second oxidation peak appeared at 460 mV and 410 mV, respectively. Most probably, there is a multistep redox reaction with the formation of a radical cation as an intermediate species, thus explaining the existence of the two pairs of reversible peaks. The intensity of the oxidation peak for NNCG1 (19.78 μA) is 17.2 times higher than that of GC (1.15 μA), the larger active surface area being the characteristic that makes NNCG1 the best-performing surface. The obtained results once again emphasise that the optimal NNCG electrode for oleuropein determination is the NNCG1 configuration, which is confirmed by the EIS studies.

3.3. Oleuropein Determination

The electrochemical response of NNCG1 to oleuropein was analysed by means of SWV measurements carried out between +0.20 and +0.70 V, with $a = 50$ mV, $f = 25$ Hz and $\Delta E_s = 2$ mV in a 0.1 M KCl solution. The analytical parameters of the developed biosensor for the determination of oleuropein, namely the linear response range, sensitivity, correlation coefficient and limit of detection, are shown in Table 3. The proposed NNCG1-based electrochemical sensor showed a linear response in the range of 5.00–500.00 μM oleuropein (Figure 7).

Table 3. The analytical parameters of the NNCG1 electrochemical sensor for the determination of oleuropein.

Linear Range (μM)	Sensitivity ($\mu\text{A } \mu\text{M}^{-1}$)	R^2	LoD (μM)
5.00–500.00	0.057 ± 0.001 *	0.9995	3.93

* Mean of 3 replicates.

The reproducibility of the developed electrochemical sensor was checked, and it was found that for seven consecutive measurements of a 100 μM oleuropein solution, the relative standard deviation (RSD) was $\pm 8.56\%$. When five different electrodes were tested under the same conditions, the RSD for electrode-to-electrode reproducibility was 11.29%. These results show that the developed NNCG1 electrochemical sensor is reproducible and stable for the analysis of oleuropein.

The analytical parameters of the developed electrochemical sensor with respect to oleuropein were compared with those from the scientific literature (Table 4), and it can be concluded that the proposed electrochemical sensor has a wide linearity range and high sensitivity compared to other sensors/biosensors. However, the limit of detection is higher than other developed oleuropein electrochemical sensors, but this is not an obstacle in the determination of OL from real samples, as the content found is relatively high.

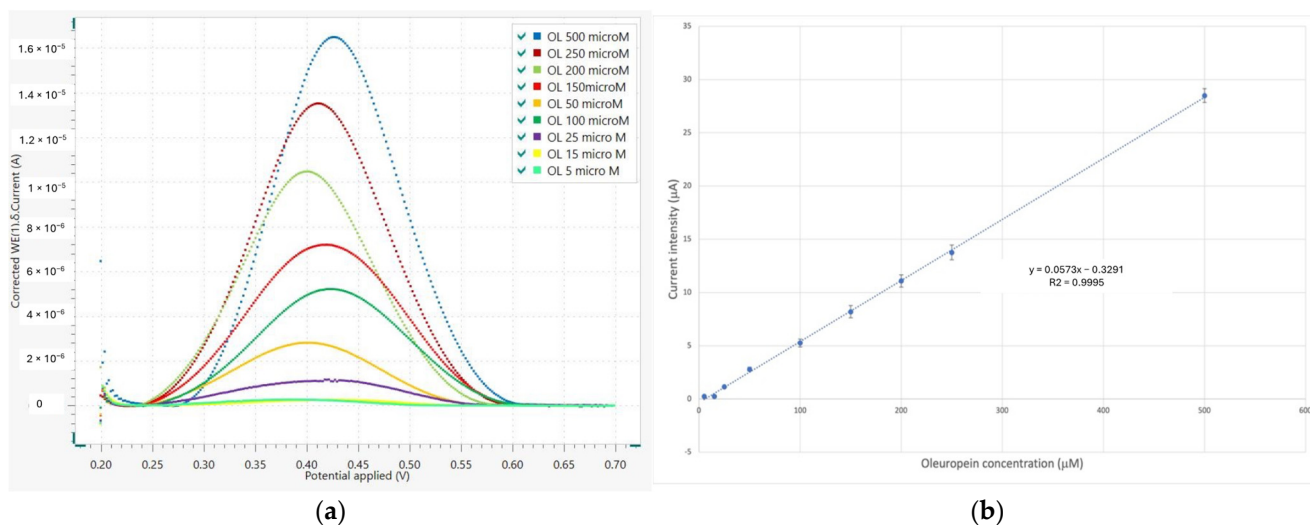


Figure 7. (a) Square wave voltammograms of different oleuropein concentrations in 0.1 M KCl solution on NNCG1 electrode: $a = 50$ mV, $f = 25$ Hz and $\Delta E_s = 2$ mV; (b) oleuropein calibration curve (3 replicates).

Table 4. The analytical characteristics of electrochemical sensors found in the literature for oleuropein determination.

Electrochemical Sensor	Electrochemical Technique	Linear Range (μM)	Sensitivity ($\mu\text{A } \mu\text{M}^{-1}$)	LoD (μM)	Reference
MWCNT/GCE	SWV	0.01–0.70	-	0.0027	[17]
LGH-GOPGE	DPV	0.10–37.00	-	0.0300	[18]
SPE/SWCNT/Lac	SWV	0.49–11.22	0.2455	0.1010	[19]
SPE/SWCNT/Tyr	SWV	0.49–11.22	0.0718	0.0953	[19]
NNCG1	SWV	5.00–500.00	0.0570	3.9300	This work

3.4. Application to EVOOs

The possibility of using the developed NNCG1 electrochemical sensor for measurements in real EVOO samples was investigated by determining the oleuropein content. The results obtained with the electrochemical sensor were compared with the results obtained using FL-HPLC as a reference method. As can be seen in Table 5, the values for oleuropein in EVOO samples obtained with the two methods are in good agreement.

Table 5. Comparison of oleuropein content obtained for EVOO samples using NNCG1 electrochemical sensor in 0.1 M KCl solution and oleuropein content obtained by FL-HPLC reference method.

EVOO	Oleuropein, μM Electrochemical Sensor	Oleuropein, μM FL-HPLC
Sotirelis EVOO, unfiltered	52.77 ± 0.80	52.16 ± 0.92
Greek local EVOO 1	231.10 ± 1.40	223.54 ± 1.70
Lidl EVOO	157.92 ± 1.20	160.72 ± 0.73
Truffle Monini EVOO	50.82 ± 0.60	49.72 ± 0.58
Monini EVOO	207.51 ± 2.30	191.78 ± 1.68
Greek local EVOO 2	11.19 ± 0.08	10.63 ± 0.33
Sotirelis EVOO	294.86 ± 3.10	297.19 ± 1.21

4. Conclusions

An electrochemical NNCG sensor with very interesting electrochemical and catalytic properties was developed, characterised and used for the determination of oleuropein in EVOO samples. The electrochemical sensor shows a very wide linear range,

5.00–500.00 μM , with an LoD of 3.93 μM and a sensitivity of 0.0570 $\mu\text{A } \mu\text{M}^{-1}$. For the determination of oleuropein in EVOOs, mainly chromatographic methods have been used so far, which require large amounts of reagents, expensive equipment and complicated procedures. Compared to chromatographic methods, the proposed electrochemical NNCG sensor is attractive due to its practicability and low cost and would be a very good alternative to the existing methods.

Author Contributions: Conceptualization, C.A., A.C., A.S., G.-L.R., A.R., M.S., O.-G.S. and S.A.V.E.; investigation, C.A., A.C., A.S., G.-L.R., A.R., M.S., O.-G.S. and S.A.V.E.; methodology, C.A., A.C., A.S., G.-L.R., A.R., M.S., O.-G.S. and S.A.V.E.; writing, C.A., A.C., A.S., G.-L.R., A.R., M.S., O.-G.S. and S.A.V.E. All authors have read and agreed to the published version of the manuscript.

Funding: This research was funded by a grant from the Ministry of Research, Innovation and Digitization, CCDI-UEFISCDI, *project number PN-III-P2-2.1-PED-2021-2256*, within PNCDI III.

Institutional Review Board Statement: Not applicable.

Informed Consent Statement: Not applicable.

Data Availability Statement: Data are contained within the article.

Conflicts of Interest: The authors declare no conflicts of interest.

References

1. Omar, S.H. Oleuropein in Olive and its Pharmacological Effects. *Sci. Pharm.* **2010**, *78*, 133–154. [[CrossRef](#)]
2. Huang, Y.L.; Oppong, M.B.; Guo, Y.; Wang, L.-Z.; Fang, S.-M.; Deng, Y.-R.; Gao, X.-M. The Oleaceae family: A source of secoiridoids with multiple biological activities. *Fitoterapia* **2019**, *136*, 104155. [[CrossRef](#)]
3. Topuz, S.; Bayram, M. Oleuropein extraction from leaves of three olive varieties (*Olea europaea* L.): Antioxidant and antimicrobial properties of purified oleuropein and oleuropein extracts. *J. Food Process.* **2022**, *46*, 15697. [[CrossRef](#)]
4. Ryu, S.J.; Choi, H.S.; Yoon, K.Y.; Lee, O.H.; Kim, K.J.; Lee, B.Y. Oleuropein suppresses LPS-induced inflammatory responses in RAW 264.7 Cell and zebrafish. *J. Agric. Food Chem.* **2015**, *63*, 2098–2105. [[CrossRef](#)] [[PubMed](#)]
5. Li, X.; Liu, Y.; Jia, Q.; LaMacchia, V.; O'Donoghue, K.; Huang, Z. A systems biology approach to investigate the antimicrobial activity of oleuropein. *J. Ind. Microbiol. Biotechnol.* **2016**, *43*, 1705–1717. [[CrossRef](#)] [[PubMed](#)]
6. Parkinson, L.; Cicerale, S. The Health Benefiting Mechanisms of Virgin Olive Oil Phenolic Compounds. *Molecules* **2016**, *21*, 1734. [[CrossRef](#)] [[PubMed](#)]
7. Zeece, M. Flavors. In *Introduction to the Chemistry of Food*; Academic Press: London, UK, 2020; pp. 213–250.
8. Hassen, I.; Casabianca, H.; Hosni, K. Biological activities of the natural antioxidant oleuropein: Exceeding the expectation—A mini-review. *J. Funct. Foods* **2015**, *18*, 926–940. [[CrossRef](#)]
9. Özcan, M.M.; Findik, S.; Aljuhaimi, F.; Ghafoor, K.; Babiker, E.F.E.; Adiamo, O.Q. The effect of harvest time and varieties on total phenolics, antioxidant activity and phenolic compounds of olive fruit and leaves. *J. Food Sci. Technol.* **2019**, *56*, 2373–2385. [[CrossRef](#)]
10. Fernández-Prior, Á.; Cardoso, J.C.; Bermúdez-Oria, A.; Reyes, Á.T.; Fernández-Bolaños, J.; Rodríguez-Gutiérrez, G. Application of a Cold-Pressing Treatment to Improve Virgin Olive Oil Production and the Antioxidant Phenolic Profile of Its by-Products. *Antioxidants* **2023**, *12*, 1162. [[CrossRef](#)]
11. Sánchez, R.; Beltrán Sanahuja, A.; Prats Moya, M.S.; Todolí, J.L. Application of Dispersive Liquid-Liquid Aerosol Phase Extraction to the Analysis of Total and Individual Phenolic Compounds in Fried Extra Virgin Olive Oils. *J. Agric. Food Chem.* **2023**, *71*, 10742–10750. [[CrossRef](#)]
12. Huang, K.; Zhong, P.; Xu, B. Discrimination on potential adulteration of extra virgin olive oils consumed in China by differential scanning calorimeter combined with dimensionality reduction classification techniques. *Food Chem.* **2023**, *405*, 134996. [[CrossRef](#)]
13. Martínez-Navarro, E.M.; Cebrián-Tarancón, C.; Moratalla-López, N.; Lorenzo, C.; Alonso, G.L.; Salinas, R.M. Development and validation of an HPLC-DAD method for determination of oleuropein and other bioactive compounds in olive leaf by-products. *J. Sci. Food Agric.* **2021**, *101*, 1447–1453. [[CrossRef](#)]
14. Carrara, M.; Kelly, M.T.; Griffin, L.; Margout-Jantac, D. Development and cross-validation of simple HPLC-fluorescence and UPLC-MS-UV methods for rapid determination of oleuropein in olive leaves. *Phytochem. Anal.* **2024**, *35*, 476–482. [[CrossRef](#)]
15. Sivakumar, G.; Briccoli Bati, C.; Uccella, N. HPLC-MS screening of the antioxidant profile of Italian olive cultivars. *Chem. Nat. Compd.* **2005**, *41*, 588–591. [[CrossRef](#)]
16. Yuan, J.J.; Tu, J.L.; Qin, F.G.F.; Xu, Y.J.; Li, B. Phenolic composition of oleuropein extract after enzymatic process by HPLC-MS and their antioxidant and antibacterial activities. *J. Food Biochem.* **2018**, *42*, 12517. [[CrossRef](#)]
17. Cittan, M.; Koçak, S.; Çelik, A.; Dost, K. Determination of oleuropein using multiwalled carbon nanotube modified glassy carbon electrode by adsorptive stripping square wave voltammetry. *Talanta* **2016**, *159*, 148–154. [[CrossRef](#)]

18. Gomez, F.J.V.; Spisso, A.; Fernanda Silva, M. Pencil graphite electrodes for improved electrochemical detection of oleuropein by the combination of Natural Deep Eutectic Solvents and graphene oxide. *Electrophoresis* **2017**, *38*, 2704–2711. [[CrossRef](#)]
19. Bounegru, A.V.; Apetrei, C. Studies on the Detection of Oleuropein from Extra Virgin Olive Oils Using Enzymatic Biosensors. *Int. J. Mol. Sci.* **2022**, *23*, 12569. [[CrossRef](#)]
20. Mohamadi, M.; Mostafavi, A.; Torkzadeh-Mahani, M. Electrochemical determination of biophenol oleuropein using a simple label-free DNA biosensor. *Bioelectrochemistry* **2015**, *101*, 52–57. [[CrossRef](#)]
21. Rojas, D.; Della Pelle, F.; Del Carlo, M.; Fratini, E.; Escarpa, A.; Compagnone, D. Nanohybrid carbon black-molybdenum disulfide transducers for preconcentration-free voltammetric detection of the olive oil o-diphenols hydroxytyrosol and oleuropein. *Microchim. Acta* **2019**, *186*, 363. [[CrossRef](#)]
22. Shekhawat, A.; Ritchie, R.O. Toughness and strength of nanocrystalline graphene. *Nat. Commun.* **2015**, *7*, 10546. [[CrossRef](#)]
23. Simionescu, O.-G.; Popa, R.C.; Avram, A.; Dinescu, G. Thin films of nanocrystalline graphene/graphite: An overview of synthesis and applications. *Plasma Process. Polym.* **2020**, *17*, e1900246. [[CrossRef](#)]
24. Gartner, M.; Anastasescu, M.; Stroescu, H.; Calderon-Moreno, J.M.; Preda, S.; Simionescu, O.-G.; Avram, A.; Buiu, O. Evolution of Nanocrystalline Graphite's Physical Properties during Film Formation. *Coatings* **2022**, *12*, 1274. [[CrossRef](#)]
25. Mani, R.C.; Sunkara, M.K.; Baldwin, R.P.; Gullapalli, J.; Chaney, J.A.; Bhimarasetti, G.; Cowley, J.M.; Rao, A.M.; Rao, K. Nanocrystalline Graphite for Electrochemical Sensing. *J. Electrochem. Soc.* **2005**, *152*, E154. [[CrossRef](#)]
26. Faggio, G.; Grillo, R.; Lisi, N.; Buonocore, F.; Chierchia, R.; Jung Kim, M.; Lee, G.-H.; Capasso, A.; Messina, G. Nanocrystalline graphene for ultrasensitive surface-enhanced Raman spectroscopy. *Appl. Surf. Sci.* **2022**, *599*, 154035. [[CrossRef](#)]
27. Wang, Y.; Cheng, M.; Wang, L.; Zhou, D.; He, S.; Liang, L.; Zhang, F.; Liu, C.; Wang, D.; Yuan, J. Nanocrystalline graphite nanopores for DNA sensing. *Carbon* **2021**, *176*, 271–278. [[CrossRef](#)]
28. Ling, T.Y.; Pu, S.H.; Fishlock, S.J.; Han, Y.; Reynolds, J.D.; McBride, J.W.; Chong, H.M.H. Sensing Performance of Nanocrystalline Graphite-Based Humidity Sensors. *IEEE Sens. J.* **2019**, *19*, 5421–5428. [[CrossRef](#)]
29. Simionescu, O.-G.; Romanitan, C.; Albu, C.; Pachi, C.; Vasile, E.; Djourelov, N.; Tutunaru, O.; Stoian, M.C.; Kusko, M.; Radoi, A. Properties of Nitrogen-Doped Nano-Crystalline Graphite Thin Films and Their Application as Electrochemical Sensors. *J. Electrochem. Soc.* **2020**, *167*, 126510. [[CrossRef](#)]
30. Albu, C.; Eremia, S.A.V.; Veca, M.L.; Avram, A.; Popa, R.C.; Pachi, C.; Romanitan, C.; Kusko, M.; Gavrilă, R.; Radoi, A. Nano-crystalline graphite film on SiO₂: Electrochemistry and electro-analytical application. *Electrochim. Acta* **2019**, *303*, 284–292. [[CrossRef](#)]

Disclaimer/Publisher's Note: The statements, opinions and data contained in all publications are solely those of the individual author(s) and contributor(s) and not of MDPI and/or the editor(s). MDPI and/or the editor(s) disclaim responsibility for any injury to people or property resulting from any ideas, methods, instructions or products referred to in the content.